# Chapter 3

# Solar distillation using three different phase change materials stored in a copper cylinder

## 3.1 Overview

In this chapter, we focus on the design and fabrication of passive solar still system with phase change materials (PCM). In order to improve the distillate, PCMs (paraffin wax, stearic acid, and lauric acid) have been stored in a copper cylinder and no extra storage facility is required to store such PCMs which further justifies the potentiality of the deployment of our solar still in uncontrolled environment. The effects of basin water depth on total distillate have been studied for all three cases. The maximum distillate has been obtained at 1 cm depth for all cases with three PCMs used in this study. Total distillate decreased linearly with water depth for all three PCMs. There has been a 9.2% drop in the maximum water basin temperature in paraffin wax as compared to stearic acid (17.6%) and lauric acid (21.5%) with an increase in water depth from 1 to 5 cm. Heat transfer and energy balance equations involved in the present solar still system have been stated. Variation of some heat transfer coefficients with time has also been studied for three different PCMs. The total distillate has been found to be increased by 1202, 1015, and 930 ml/$m^2$-day for paraffin wax, stearic acid, and lauric acid, respectively stored in a copper cylinder. The performance of lauric acid for total distillate has been comparable with the other two PCMs.

## 3.2 Materials and Methods

### 3.2.1 Experimental setup and procedure

The schematic and vivid description of the experimental system is shown in Fig. 3.1. The single slope solar still (75 cm × 75 cm × 15 cm) is made of stainless steel thickness of 1 mm mounted with copper cylinder loaded with PCM. The PCM loaded copper cylinders have been placed in a basin of solar still at a proper distance. In the present study, 1.32 kg of PCM stored in 6 copper

cylinders of 7 cm height and 7 cm diameter have been found to be appropriate for providing larger surface area for the given amount of PCM which can be considered enough for complete melting under the paradigm of efficient energy storage. Different experiments have been performed in the variation of water depth (1–5 cm) coupled with different PCMs. The thermo-physical properties of three PCMs used, including their melting and solidifying range is depicted in Table 3.1 (Farid et al., 2004; Sharma et al., 2009; Zalba et al., 2003). The experimental parameters involved in the study have been given in Table 3.2. As depicted in Fig. 3.1, each copper cylinder has been allowed to fill fully and sealed with high temperature rubber cork.

**Table 3.1** Thermo-physical properties of PCM (Farid et al., 2004; Sharma et al., 2009; Zalba et al., 2003)

| **Material properties** | **Lauric acid** | **Stearic acid** | **Paraffin wax** |
|---|---|---|---|
| **Chemical formula** | $(CH_3(CH_2)_{10}COOH)$ | $(CH_3(CH_2)_{16}COOH)$ | $(C_{31}H_{64})$ |
| **Melting temperature, $^oC$** | 42-46$^oC$ | 52-56$^oC$ | 58-60$^oC$ |
| **Latent heat of fusion kJ/kg** | 178 | 199 | 226 |
| **Solid density, kg/m$^3$** | 862 | 847 | 818 |
| **Thermal conductivity, W/m-$^oC$** | 0.16 | 0.290 | 0.24 |
| **Specific heat capacity, kJ/kg $^oC$** | 2.1 | 1.590 | 2.95 |

**Table 3.2** Experimental parameters

| Parameters | Symbols | Value |
|---|---|---|
| **Transmittance of cover** | $\tau_c$ | 88% |
| **Emissivity of cover** | $\varepsilon_c$ | 0.97 |
| **Wind velocity** | V | 1 m/s |
| **Density of water** | $\rho$ | 989 kg/m$^3$ |
| **Latent heat of vaporization** | $h_{fg}$ | 2372 (KJ/kg) |
| **Declination angle** | $\delta$ | 32$^o$ |
| **Latitude of Varanasi** | $\varphi$ | 25.31$^o$ |

**Table 3.3** Accuracies and range for various instruments

| S. No. | Instrument | Accuracy | Range |
|---|---|---|---|
| **1** | **Solar power meter** | 10 W/m$^2$ | 0 - 1999 W/m$^2$ |
| **2** | **Digital thermocouple** | ± 1$^o$C | -50 - 110$^o$C |
| **3** | **Measuring jar** | ± 10 ml | 0-2000 ml |
| **4** | **Anemometer** | 2-4 | 0.4-30 m/s |
| **5** | **Hygrometer**<br>**Ambient temperature**<br>**Relative humidity** | <br>± 1$^o$C<br>± 10 | <br>-50 - 70$^o$C<br>10-99% |
| **6** | **TDS meter** | ±2% | 0-5000 ppm (mg/l) |

**Table 3.4** Equation parameters obtained by curve fitting of distillate vs depth of water

| PCM | Paraffin wax | Stearic acid | Lauric acid |
|---|---|---|---|
| **Residual sum of squares** | 5143.9 | 4359.1 | 9294.3 |
| **Pearson's r** | -0.9931 | -0.99177 | -0.98754 |
| **$R^2$** | 0.98625 | 0.9836 | 0.97523 |
| **Adj. $R^2$** | 0.98167 | 0.97814 | 0.96698 |
| **Linear equation** | **Y**= -(192.1±13.094)**X** + (2683.3±43.423) | **Y**= (-161.7±12.054)**X** + (2487.1±39.978) | **Y**= (-191.3±17.601)**X** + (2437.3±58.377) |

*where Y is total distillate and X is depth of water

The experiments have been conducted in the month of October from 09.00 am to 08.00 pm. The hourly variation of temperatures have been noted by using P-T 100 thermometers at different points in the solar still. In addition, solar intensity has been measured using solar power meter at the parallel surface of the solar still (accuracy and range of various instruments used in this experiment have been shown in Table 3.3).

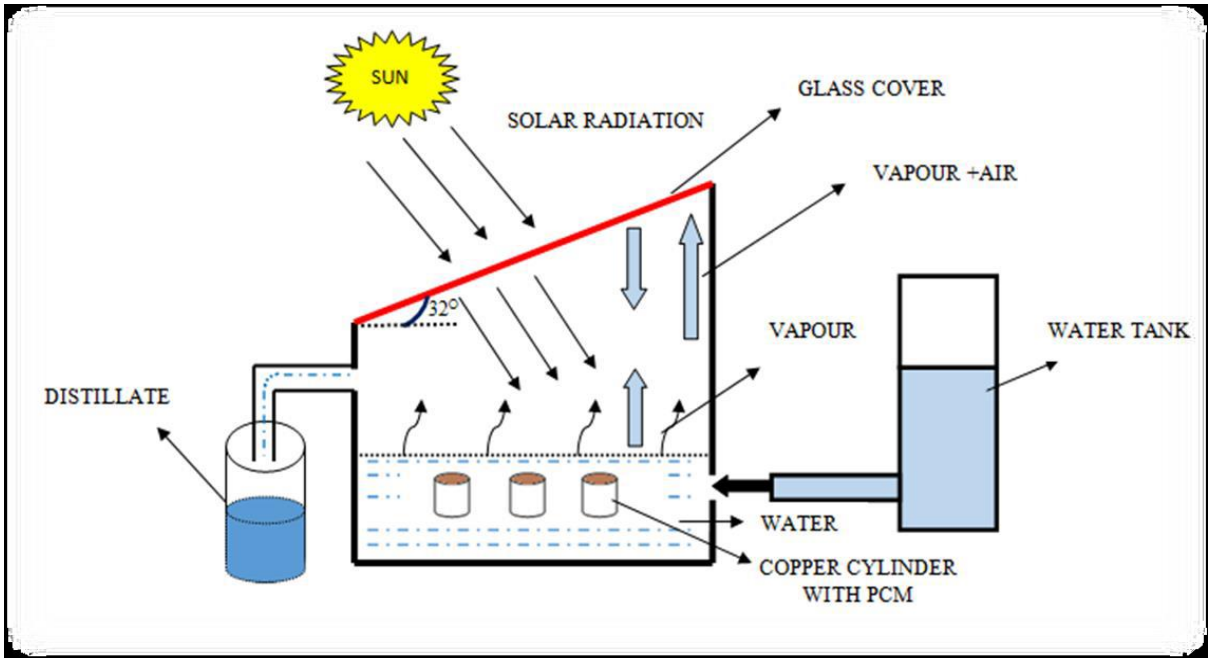


**Fig. 3.1** Schematic diagram of passive solar still with PCM

**Fig. 3.2** Pictorial view of the experimental setup for solar still coupled with PCM stored in copper cylinder

**Fig. 3.3** Pictorial view of PCM loaded copper cylinders


**Fig. 3.4** PCMs used in the experiment

Fig. 3.2 represents the pictorial view of the experimental set-up used in the present study. Copper cylinders, as depicted in Fig. 3.3, have been used to store different types of PCMs in order to improve the overall performance due to its higher conductivity, non-corrosive, longer durability, and nontoxic in nature. A commercial grade of lauric acid, stearic acid, and paraffin wax have been used as represented in Fig. 3.4.

### 3.2.2 Principles of operation

It can be attributed to Fig. 3.1 that during charging mode the solar radiation is transmitted through the glass cover, and it is absorbed by the copper cylinder and basin liner resulting in temperature rise. All six copper cylinders in each case have been filled with 1.3 kg of PCM. A part of the energy absorbed by the basin liner as represented in Fig. 3.1 is transmitted through convection to the basin water. The copper cylinders are heated due to solar radiation and convective heat transfer from water during the charging mode. Heat is first stored as a sensible heat until the PCM reaches its melting point. At this time, PCM starts to melt, resulting in heat storage in the form of latent heat, and after the complete melting of the PCM, the heat will be stored in the melted PCM as sensible heat. After the sunset (discharging mode), when the solar radiation is zero, the still components start to cool down and the liquid PCM transfers heat to the copper cylinder through conduction mode and from copper cylinder to the basin water through convective mode until the PCM completely solidified and equilibrium temperature is

achieved by all components of the solar still. The PCM acts as a heat source for the basin water during the absence of solar intensity. As a consequence, the still continue to produce pure water as collected in the bottle represented in Fig. 3.1 even after sunset.

## 3.3 Heat transfer and energy balance

Heat transfer in solar still loaded with PCM inside copper cylinder generally depends upon energy transfer between basin liners, basin water, copper cylinder, PCM and glass cover. Solar energy trapped inside the solar still during charging and discharging mode witnesses some losses through glass cover (El-Samadony et al., 2016; Singh and Tiwari, 1993). Heat loss through glass cover occurs mainly in the form of convective, radiative, and evaporative mode. The convective ($h_{cwg}$), radiative ($h_{rwg}$), and evaporative ($h_{ewg}$) heat transfer coefficients can be calculated using Dunkle (Dunkle, 1961) correlations. There have been some assumptions made while considering the heat transfer mechanism and energy balance equations. These are as follows:

1. The heat capacities are negligible for basin liner, glass cover, insulating material and copper cylinder as compared to basin water and PCM.

2. Heat transfer from basin liner to the copper cylinder and copper cylinder to glass cover is neglected.

3. The system is considered vapour tight with completely insulated and the side losses are neglected and hence, any effect of the vapor pressure of the PCMs vapor generated in the copper tube has not been considered.

4. Heat transfer inside the copper cylinder and PCM is predominantly due to conduction. This is due to the fact that convection does not take place within the copper cylinder when PCM is melted.

5. For simplicity, no thermal gradient is considered throughout the PCM, and its average temperature has been used for all calculations.

### 3.3.1 Heat loss due to convective heat transfer

The convective mode of heat transfer depends strongly on fluid properties, heat conduction, and slow characteristics. In solar still system coupled with PCM witness convection heat transfer between the water basin surface, and the inner glass cover surface through humid air existing due to temperature difference between them. The convection rate of heat transfer inside the solar still can be calculated using Eq. (3.1) and is expressed in terms of water temperature (Tw) and glass inner surface temperature ($T_{gi}$).

$$Q_{Cwg} = h_{Cwg} \times (T_w - T_{gi}) \quad (3.1)$$

Where $h_{cwg}$ is the convective heat transfer coefficient from water to the inner surface of the glass cover, and it can be calculated by Eq. (3.2) as expressed in Dunkle (Dunkle, 1961)correlations.

$$h_{cwg} = 0.884\left\{(T_w - T_{gi}) + \frac{[P_w - P_{gi}][T_w + 273.15]}{[268900 - P_w]}\right\}^{\frac{1}{3}} \quad (3.2)$$

,where $P_w$ and $P_{gi}$ can be calculated using Eqs. (3.3) and (3.4) Dunkle (Dunkle, 1961) and Chen et al. (Chen et al., 2013):

$$P_w = exp^{\left(25.317 - \frac{5144}{T_w + 273}\right)} \quad (3.3)$$

$$P_{gi} = exp^{\left(25.317 - \frac{5144}{T_g + 273}\right)} \quad (3.4)$$

### 3.3.2 Heat loss due to radiative heat transfer

The mechanism involved during the thermal mode of heat transfer includes the emission of internal energy by the object. In the present solar still system, heat transfer due to thermal radiation occurs between the water and inner glass surface separated by medium colder than

both bodies. The inclination of glass cover with respect to the water basin is small due to which the view factor between these two surfaces is considered unity. The radiative heat transfer rate ($h_{rwg}$) between glass cover surface and water can be calculated by Eq. (3.5) Dunkle (Dunkle, 1961) and Chen et al. (Chen et al., 2013):

$$Q_{rwg} = h_{rwg} \times (T_w - T_{gi}) \tag{3.5}$$

,where $h_{rwg}$ is the radiative heat transfer coefficient between the glass cover inner surface and water mass evaluated by Eq. (3.6):

$$h_{rwgi} = \varepsilon_{eff}\sigma\left[(T_w + 273)^2 + \left(T_{gi} + 273\right)^2\right]\left(T_w + T_{gi} + 546\right) \tag{3.6}$$

The effective remittance between glass cover and water mass is given as in Eq. (3.7):

$$\varepsilon_{\text{eff}} = \left(\frac{1}{\varepsilon_{\text{w}}} + \frac{1}{\varepsilon_{\text{g}}} - 1\right)^{-1} \tag{3.7}$$

### 3.3.3 Heat loss due to evaporative heat transfer

The vapour pressure is lower as compared to the saturation pressure of the liquid at given temperature evaporation happens between the vapour–liquid interfaces. The evaporative heat transfer occurs between water vapour and water interface (Chen et al., 2013; Dunkle, 1961) the rate of evaporative heat transfer can be expressed as in Eq. (3.8):

$$Q_{ewg} = h_{ewg} \times (T_w - T_{gi}) \tag{3.8}$$

,where, $h_{ewg}$ is evaporation heat transfer coefficient between water mass and inner surface of glass cover, and it can be calculated by Eq. (3.9):

$$h_{ewg} = 13.273 \times 10^{-3} \times h_{Cwg} \times \left[\frac{P_w - P_{gi}}{T_w - T_{gi}}\right] \tag{3.9}$$

The total heat transfer rate ($Q_{twg}$) can be expressed as in Eq. (3.10) and (3.11):

$$Q_{twg} = Q_{Cwg} + Q_{rwg} + Q_{ewg} \quad (3.10)$$

Here, $Q_{twg} = h_{twg} \times (T_w - T_{gi})$ (3.11)

The total internal heat transfer coefficient between the water mass and the inner surface of glass cover ($h_{twg}$) can be calculated as given in Eq. (3.12):

$$h_{twg} = h_{Cwg} + h_{rwg} + h_{ewg} \quad (3.12)$$

The conductive heat transfer rate through the glass cover thickness from its inner surface to the outer surface can be expressed as in Eq. (3.13):

$$Q_{cdgi-go} = \frac{K_g}{L_g}\left(T_{gi} - T_{go}\right) \quad (3.13)$$

### 3.3.4 Solar still with PCM (charging mode)

In the present solar still system during the charging mode, heat transfer occurs between the water basin, and copper cylinder and the energy balance equation during the sunshine hours may be expressed as in Eq. (3.14):

$$h_{lw}A_1(T_l - T_w) + I\tau_g\alpha_w A_1 = A_1 h_t\left(T_w - T_g\right) + h_{wc}A_2(T_w - T_c) + m_w C_w \frac{dT_w}{dt} \quad (3.14)$$

,where, $A_1$ is the area of the water basin, and $A_2$ is an area of contact between water and copper cylinder.

On the basis of stated assumptions in Section 3.2.4. The energy balance between basin liner and water can be expressed as in Eq. (3.15):

For basin liner (considering no heat loss to through insulation)

$$I\tau_g\tau_w\alpha_l = h_{lw}(T_l - T_w) \quad (3.15)$$

During the charging mode, heat transfer occurs between PCM and water basin via copper cylinder. The energy balance equation for the copper cylinder is given by Eq. (3.16):

$$I\tau_g\alpha_c A_3 + h_{wc}A_2(T_w - T_c) = A_4\frac{K_c}{X_c}\left(T_c - T_{pcm}\right) \quad (3.16)$$

,where $A_3$ is cross-sectional area, and $A_4$ is the total surface area of the copper cylinder. PCM during the charging mode stores solar energy in the form of sensible heat and latent heat of fusion. On the basis of assumptions made, the heat transfer between PCM and copper cylinder occurs mainly due to conduction, and energy balance for PCM can be expressed as in Eq. (3.17):

$$A_4 \frac{K_c}{X_c}\left(T_c - T_{pcm}\right) = M_E \frac{dT_{pcm}}{dt} \qquad (3.17)$$

,where $M_E$ is the equivalent heat capacity and can be expressed as:

$M_E = m_{pcm} C_s$ for $T_{pcm} < T_m$

$M_E = m_{pcm} L_s$ for $T_{pcm} = T_m$

$M_E = m_{pcm} C_l$ for $T_{pcm} > T_m$

### 3.3.5 Solar still with PCM (discharging mode)

In the absence of solar radiation as the temperature of the water, basin decreases, solidification (phase change) of PCM happens to result in net heat transfer from PCM to water basin via copper cylinder. As the temperature difference between liner and water basin is negligible during discharging mode; hence, heat transfer between them can be neglected.

Based on assumptions made, the energy balance equations for water basin during Sunset hours can be expressed as in Eq. (3.18):

$$h_{wc} A_2 (T_c - T_w) = A_1 h_t \left(T_w - T_g\right) + m_w C_w \frac{dT_w}{dt} \qquad (3.18)$$

Here, the heat transfer between liner and water is negligible during sunset hours. For the basin liner, the heat transfer is zero during discharging mode as we have considered no heat loss from the liner base to insulation.

The energy balance equation for copper cylinder during discharging mode can be given by Eq. (3.19):

$$A_4 \frac{K_c}{X_c}\left(T_{pcm} - T_c\right) = h_{wc} A_2 (T_c - T_w) \quad (3.19)$$

During sunset hours heat transfer occurs from PCM to copper cylinder, and as a convective mode of heat transfer between them can be neglected, the energy balance equation for PCM is given by Eq. (3.20):

$$M_E \frac{dT_{pcm}}{dt} = A_4 \frac{K_{pcm}}{X_{pcm}}\left(T_{pcm} - T_c\right) \quad (3.20)$$

,where, $M_E$ is the equivalent heat capacity and can be expressed as:

$M_E = m_{pcm} C_s$ for $T_{pcm} < T_m$

$M_E = m_{pcm} L_s$ for $T_{pcm} = T_m$

$M_E = m_{pcm} C_l$ for $T_{pcm} > T$

## 3.4 Results and discussion

### 3.4.1 Variation of solar intensity, ambient temperature and glass cover temperature with time

The solar still performance with the phase change materials has been studied in the month of October when the intensity of solar radiation is low as compared to summer. Fig. 3.5 depicts the variation of solar radiation and ambient temperature with respect to the time, and average values have been quoted for the course of five different depth of water for respective PCMs. In this study $I_L$, $I_S$, and $I_P$ represents solar intensity for lauric acid, stearic acid and paraffin wax, respectively. $T_{aL}$, $T_{aS}$, and $T_{aP}$ show the ambient temperature for lauric acid, stearic acid, and paraffin wax, respectively. Fig. 3.6 represents the glass cover temperatures ($T_g$) for three different PCMs, and average values have been stated in this study for the course of five

different depths. It can be illustrated that glass temperature increases with time and reaches a maximum temperature between 01:00–2:00 PM. It has been obvious that in the early hours of the day the inner glass temperature is close to that of water basin temperature. However, as the day, progresses the difference increases due to the fact that water can absorb some of the incident solar energy, whereas glass transmits most of the incident solar intensity.

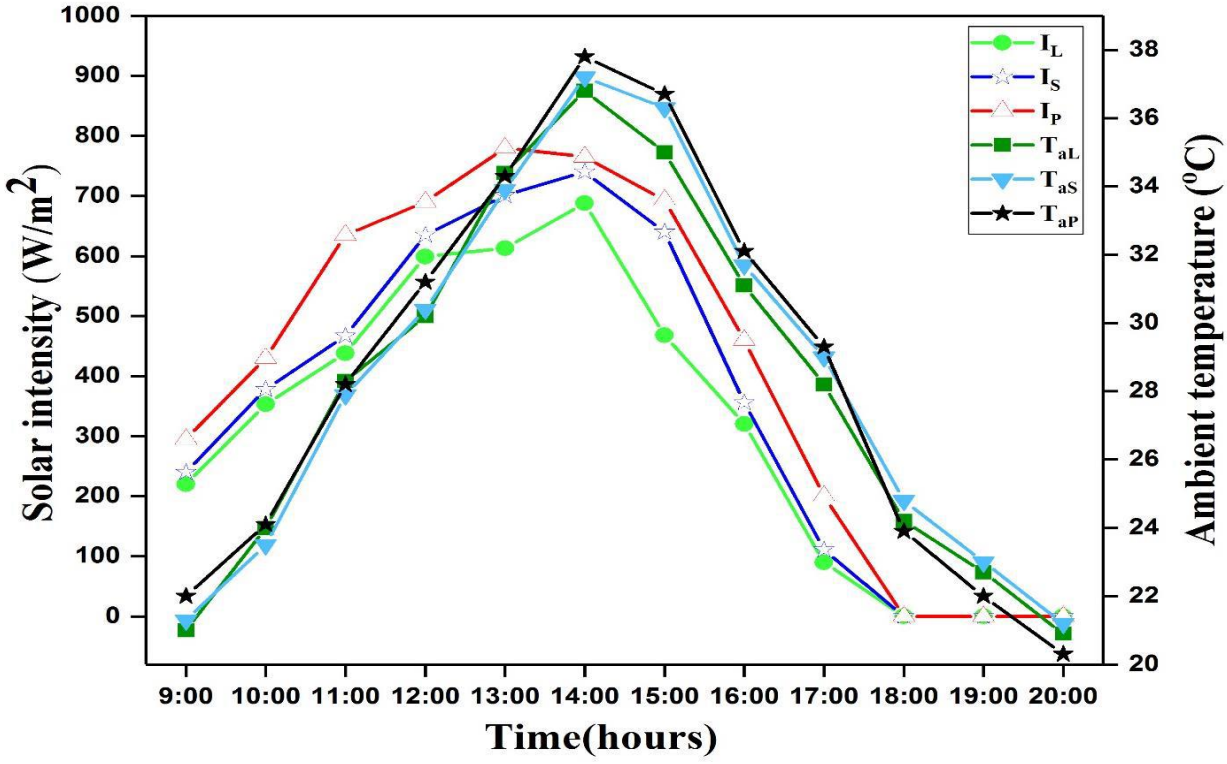


**Fig. 3.5** Solar intensity and ambient temperature variation for different PCMs with respect to time

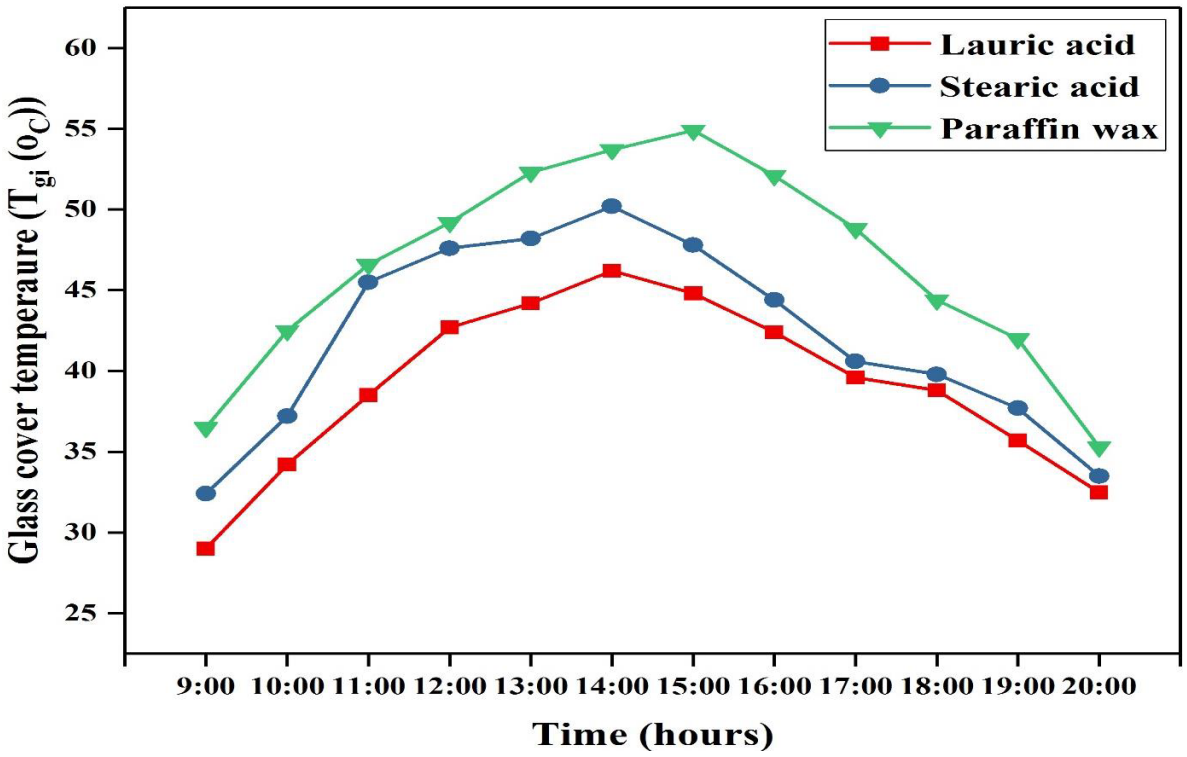


**Fig. 3.6** Variation of glass cover temperature for three different PCMs with respect to time

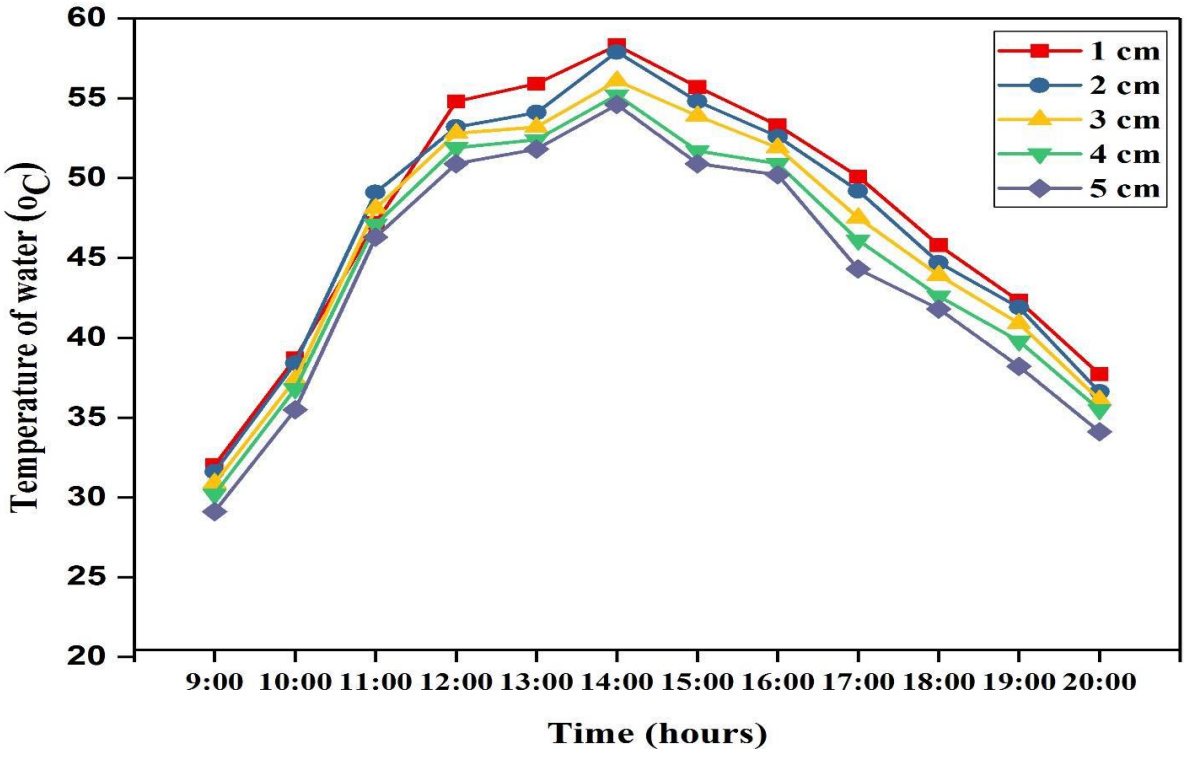


**Fig. 3.7** Temperature of water basin coupled with lauric acid

### 3.4.2 Variation of water basin temperature with depth of water

In Figs. 3.7, 3.8 and, 3.9, it can be noted that the maximum average temperature attained by the water basin decreases with an increase in depth of water. It can also be observed that for paraffin wax there has been 9.2% drop in the maximum water basin temperature as compared to stearic acid (17.6%) and lauric acid (21.5%) when the water depth has been increased from 1 cm to 5 cm. The decrease in water basin temperature with an increase in depth of water has been due to the fact that the amount of water in the basin increased.

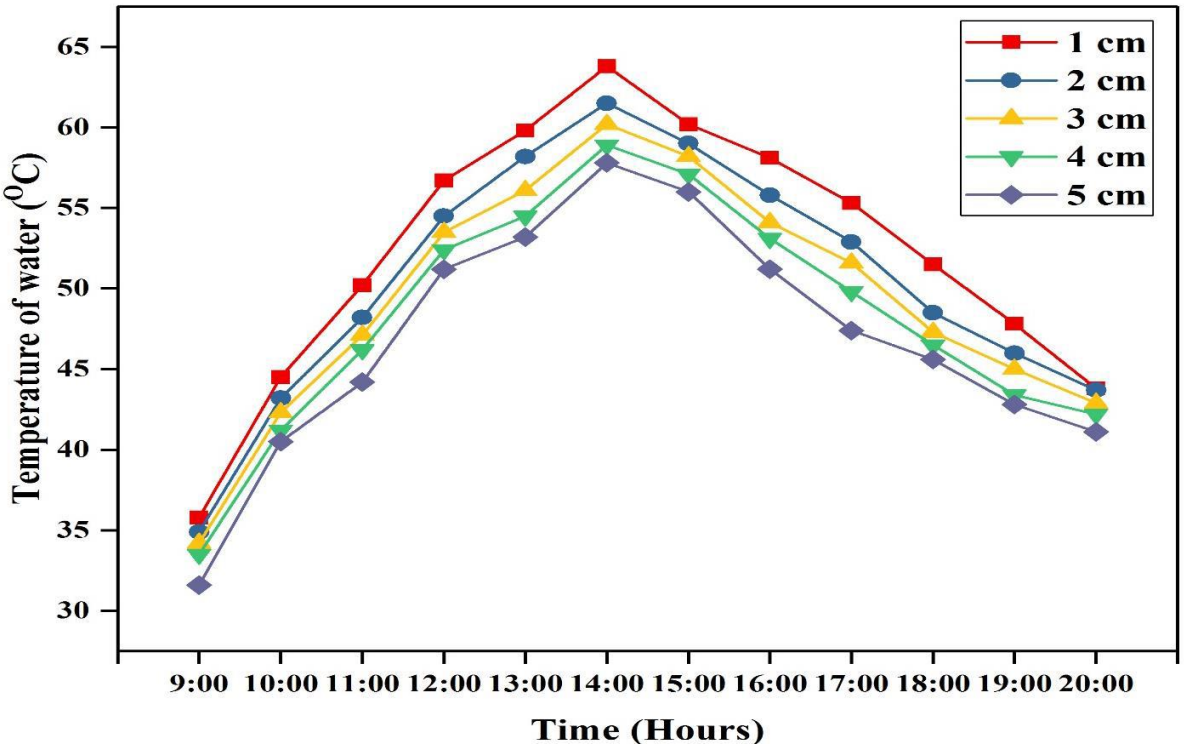


**Fig. 3.8** Temperature of water basin coupled with stearic acid

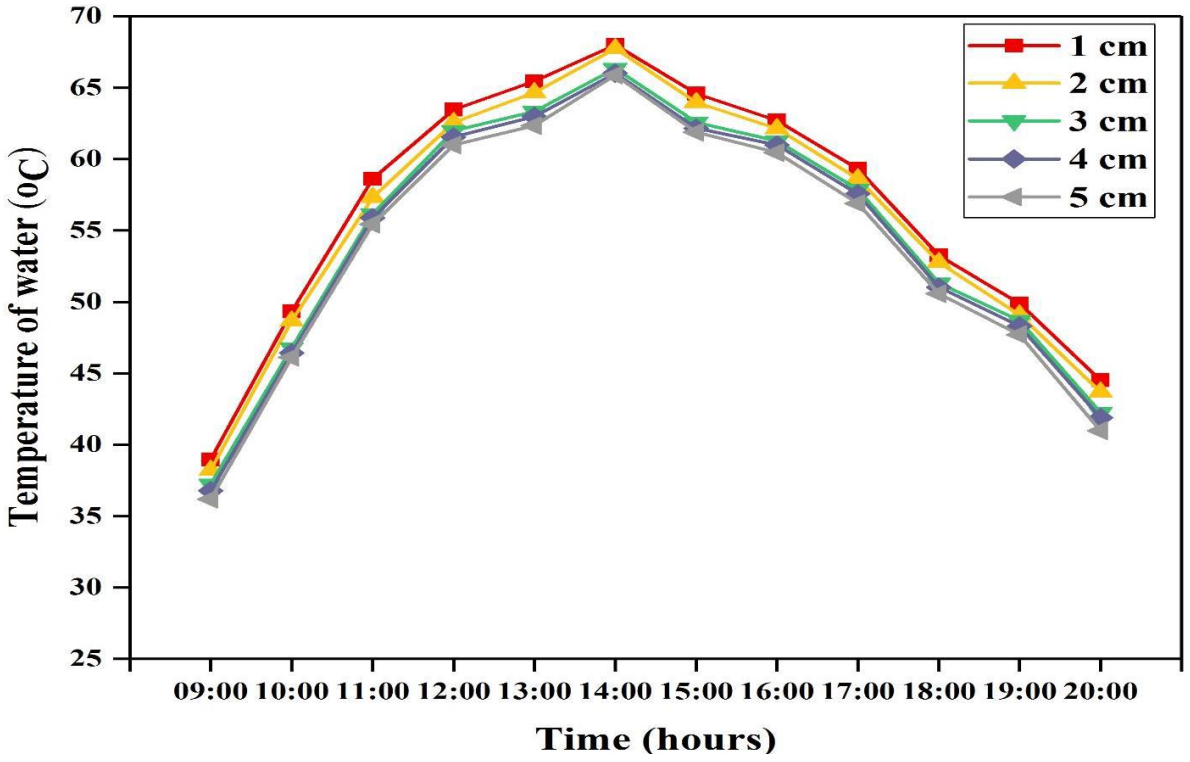


**Fig. 3.9** Temperature variation of water basin coupled with paraffin wax

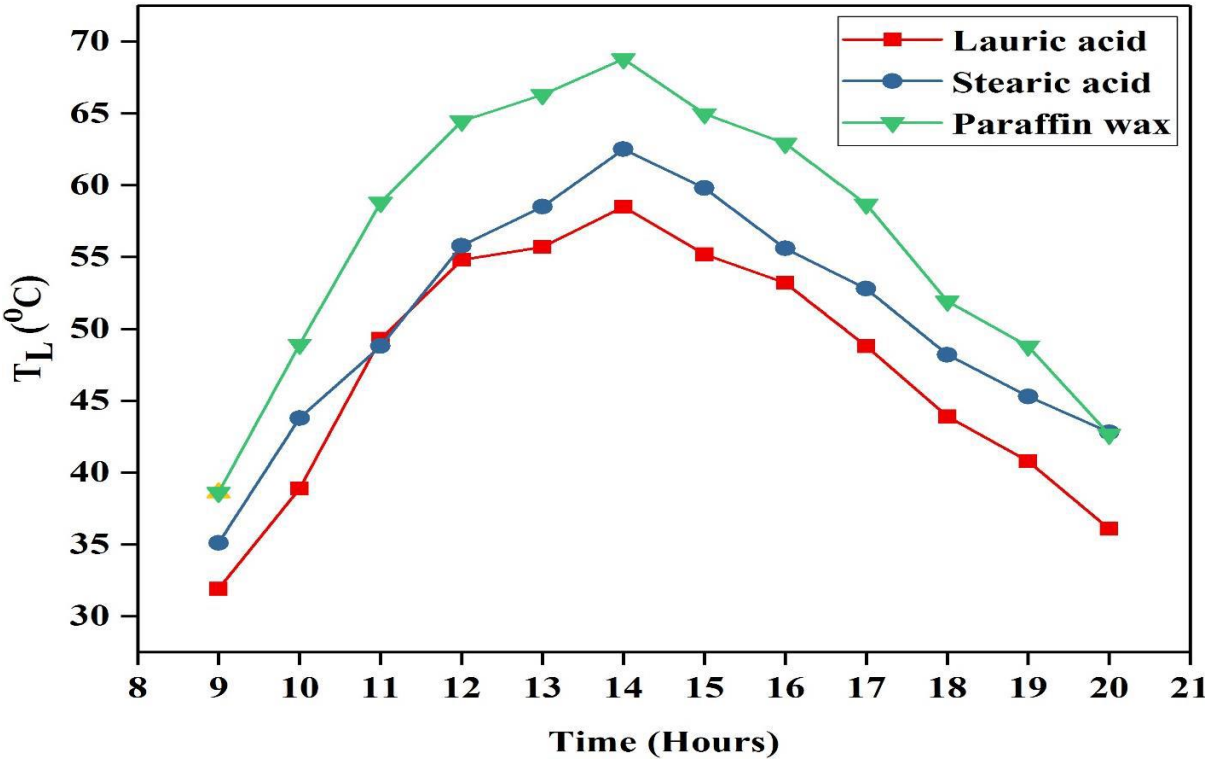


**Fig. 3.10** Temperature variation of liner for three different PCMs

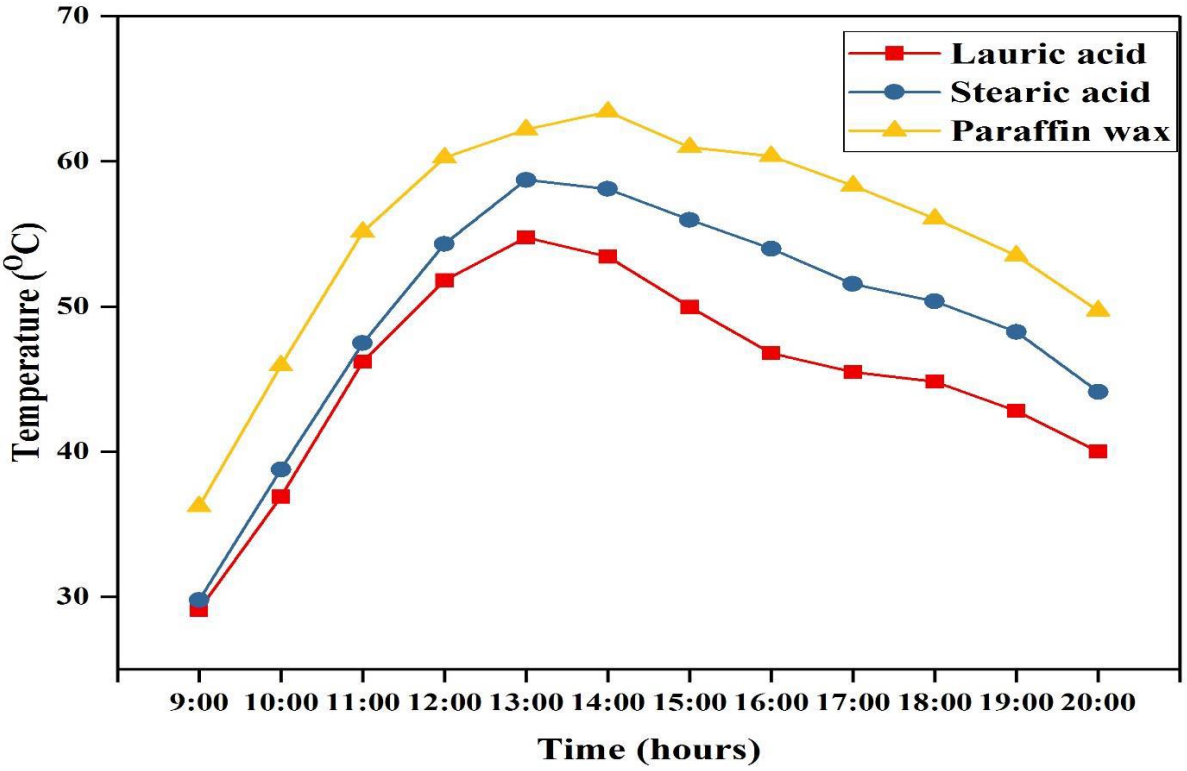


**Fig. 3.11** hourly temperature variation of PCMs

During the sunshine hours when solar intensity increases the temperature of PCM also increase and subsequently decrease when comparatively lower solar intensities are available. That is why, there is a peak in Fig. 3.11 and after that during sunset hours there is a decrease in temperature of PCMs. Moreover, in sunset hours due to lack of radiation, the temperature of water in the basin decreases slowly due to the use of stored heat energy from the PCM. The variation between water basin temperatures in all three cases at different water depths has also been due to some environmental conditions like fluctuation in solar radiation, wind speed, ambient temperature, and spatial wind barriers.

As the day progresses in the first half, water temperature increases faster as compare to the glass temperature due to expose of glass surface to the ambient atmosphere. Alteration in glass and water temperature can be attributed to unstable climatic conditions. However, in all cases, the pattern followed by the curves in Figs. 3.6, 3.7, 3.8, and 3.9 have a similarity.

### 3.4.3 Temperature variation of PCM and basin liner

The hourly variation of liner temperature for different PCMs has been represented in Fig. 3.10. The average maximum temperature over the course of five different depths has been 68.8, 62.5, and 58.5 $^{o}$C for paraffin wax, stearic, and lauric acid, respectively. Basin liner has been painted black for the fact that it can absorb maximum incident solar radiation after some of the radiation is lost through glass cover while some have been absorbed by the water basin.

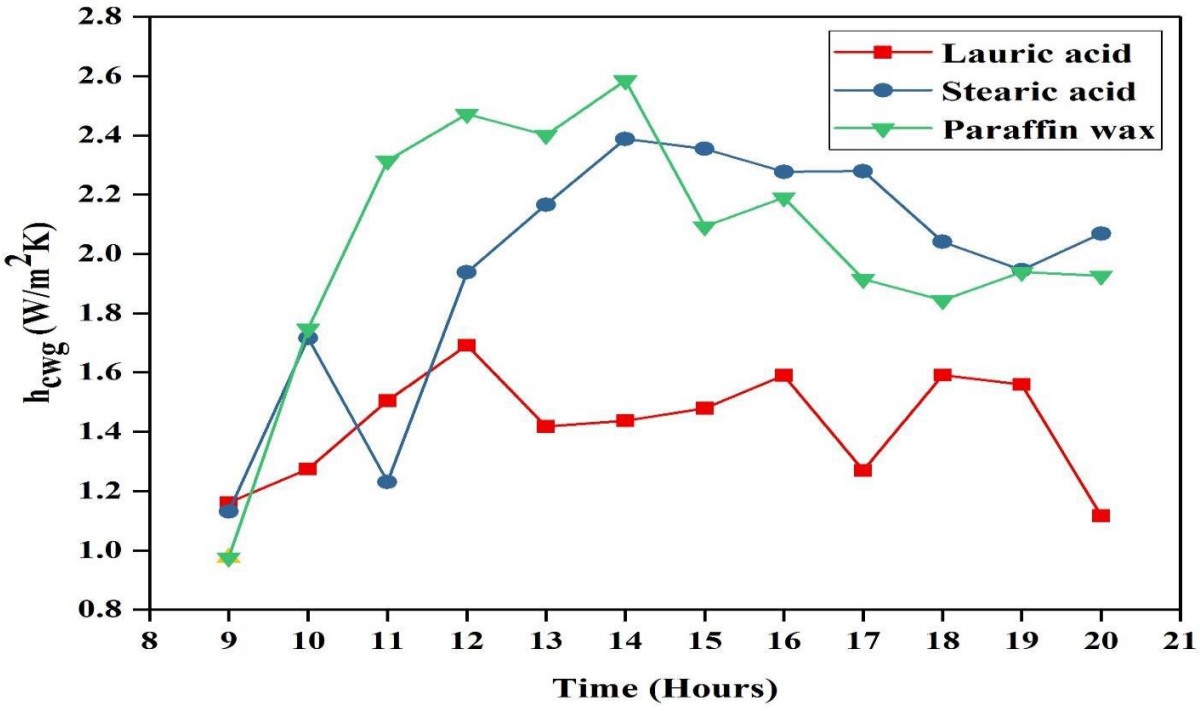


**Fig. 3.12** Convective heat transfer coefficient from water to glass cover with respect to time

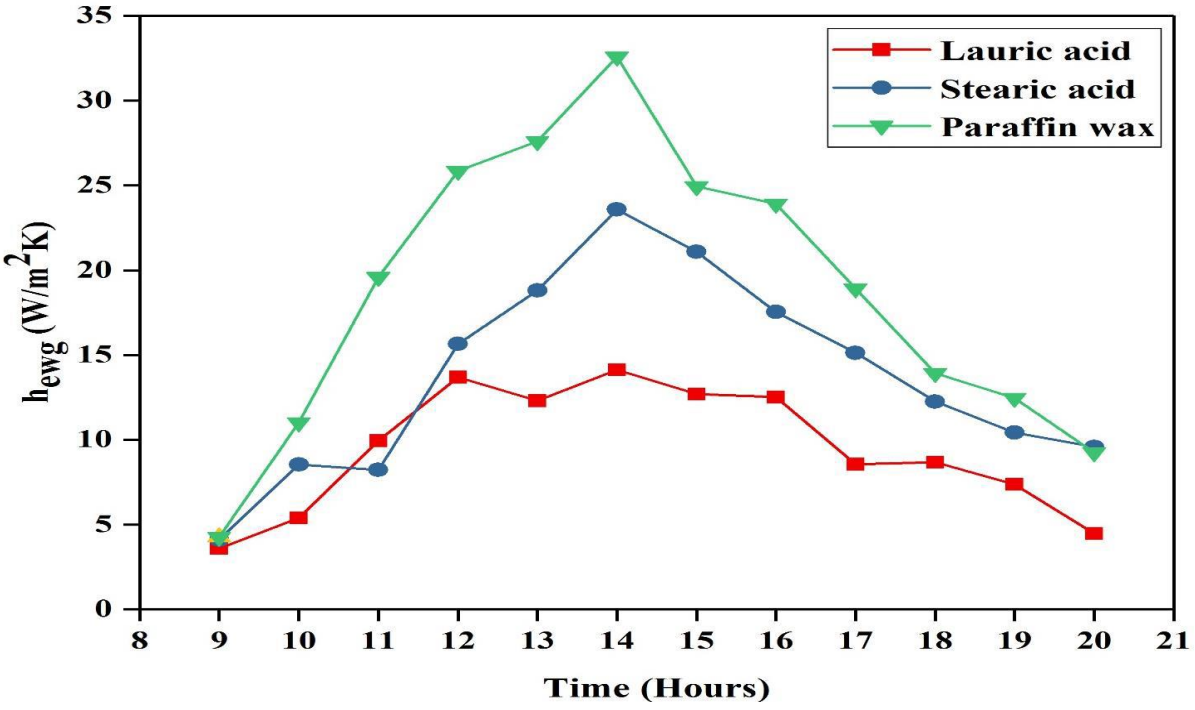


**Fig. 3.13** Evaporative heat transfer coefficient from water to glass cover with respect to time

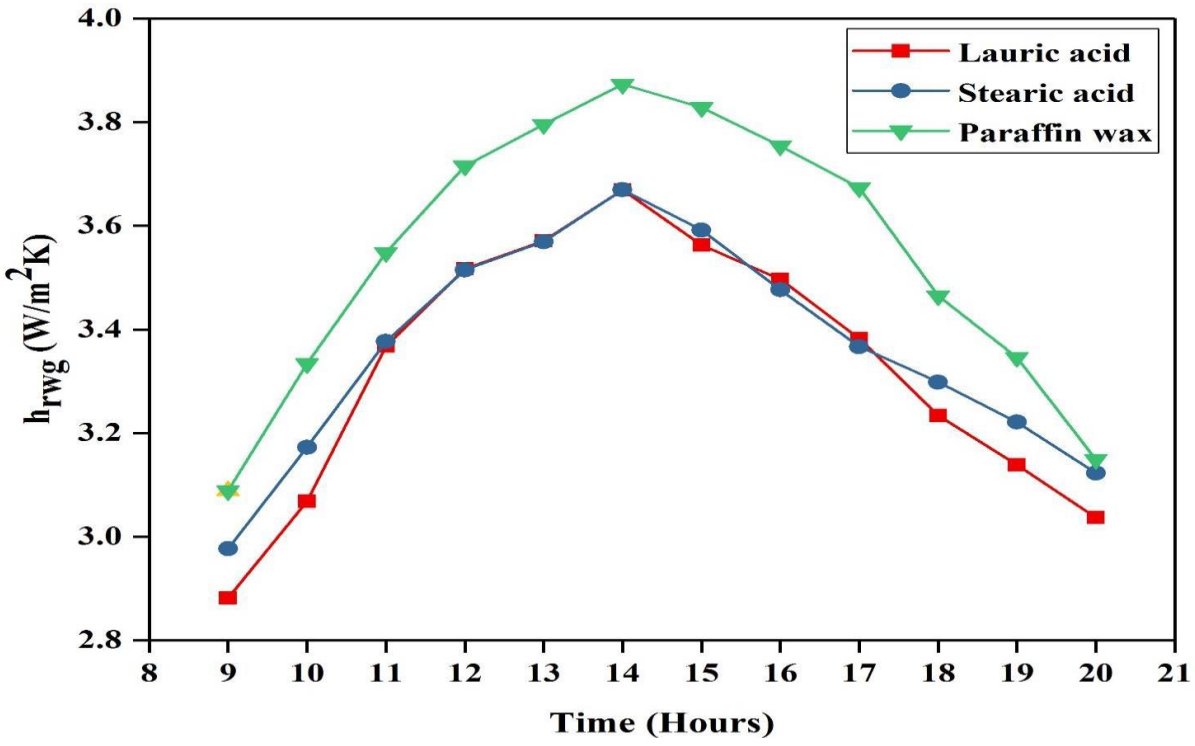


**Fig. 3.14** Radiative heat transfer coefficient from water to glass cover with respect to time

Fig. 3.11 indicates PCM temperature for three different PCMs. It can be observed that $T_{PCM}$ increases with time as the solar radiation increases. Sensible heat is stored in the form of

thermal energy in the solid PCM until it reaches the melting point. The melting point of paraffin wax is about 59 $^{o}$C, whereas for lauric and stearic acid, it is about 44 $^{o}$C and 54 $^{o}$C, respectively. Then $T_{PCM}$ continues to be constant for some time interval during the noontime as the PCM undergoes phase transformation. Once complete phase transformation occurs, the TPCM again increases due to sensible heat storage in liquid form. Maximum temperature achieve by PCMs have been 53.4 $^{o}$C (lauric acid), 58.1 $^{o}$C (stearic acid) and 63.4 $^{o}$C (paraffin wax). As the temperature increased beyond the melting point in all three cases confirmed that the complete melting of PCMs occurred during the experiment. However, (Tabrizi et al., 2010) observed in their study that the complete melting of PCM did not occur and this suggests that in our study, the PCMs have been stored in copper cylinders resulted in better heat transfer. It can also be observed that once the discharging process started at constant temperature unless PCM completely solidified and afterwards $T_{PCM}$ decreases gradually with time in all three cases. It is seen that the $T_{PCM}$ increases with time due to the increased rate of heat transfer by conduction from the basin liner to the PCM as the solar radiation intensity increases. The PCM starts melting after achieving its melting point temperature from exposure to solar radiation at a higher level. Afterwards, $T_{PCM}$ decreases slowly with time after sunset when the discharging process of heat stored within the PCM begins.

### 3.4.4 Variation of heat transfer coefficient for different PCMs

It can be observed from Figs. 3.12–3.16, that heat transfer coefficient ($h_{cwg}$, $h_{ewg}$, $h_{rwg}$, $h_t$, and $h_{lw}$) varies with time for all solar still components. In this study, we have calculated the heat transfer coefficient for water to glass during the observed period as most of the losses in the solar still occurs through glass cover (as no heat loss is considered from insulation side).

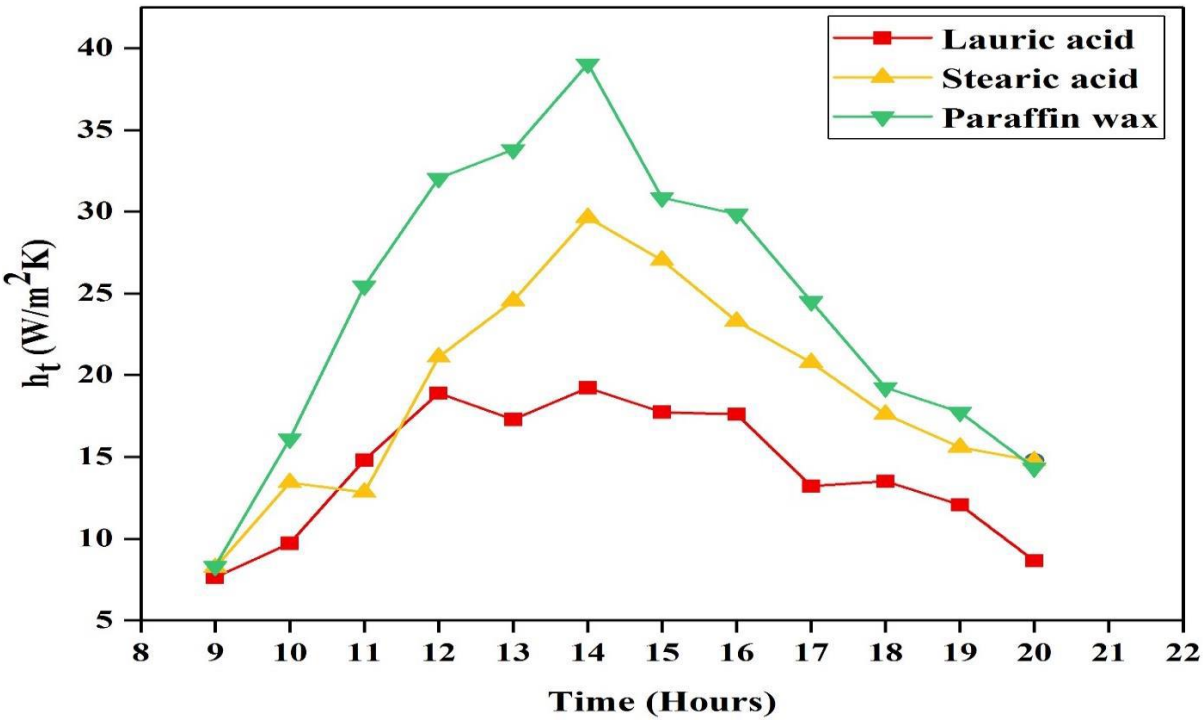


**Fig. 3.15** Total heat transfer coefficient from water to glass cover with respect to time

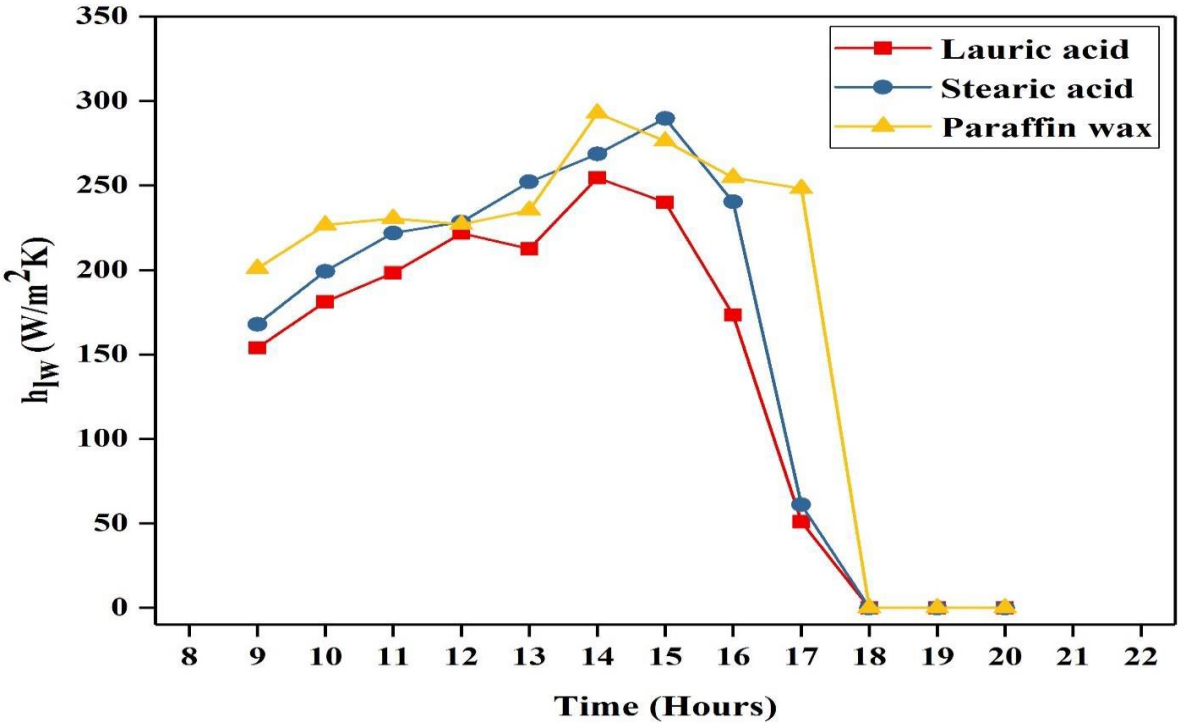


**Fig. 3.16** Heat transfer coefficient from liner to water with respect to time

In Figs. 3.12–3.15, the heat transfer coefficient is more for paraffin wax followed by stearic acid and lauric acid due to the fact that incident solar radiation in case of paraffin wax has been higher and the temperature difference between glass cover temperature, and water is less during

the charging mode. There was no proper trend followed in the case of the heat transfer coefficient from liner to water due to the fact that there has been no influence of PCM property on heat transfer mechanism occurring between liners to water. After sunset, as the temperature of liner and water becomes approximately equal, the heat transfer coefficient ($h_{lw}$) becomes zero.

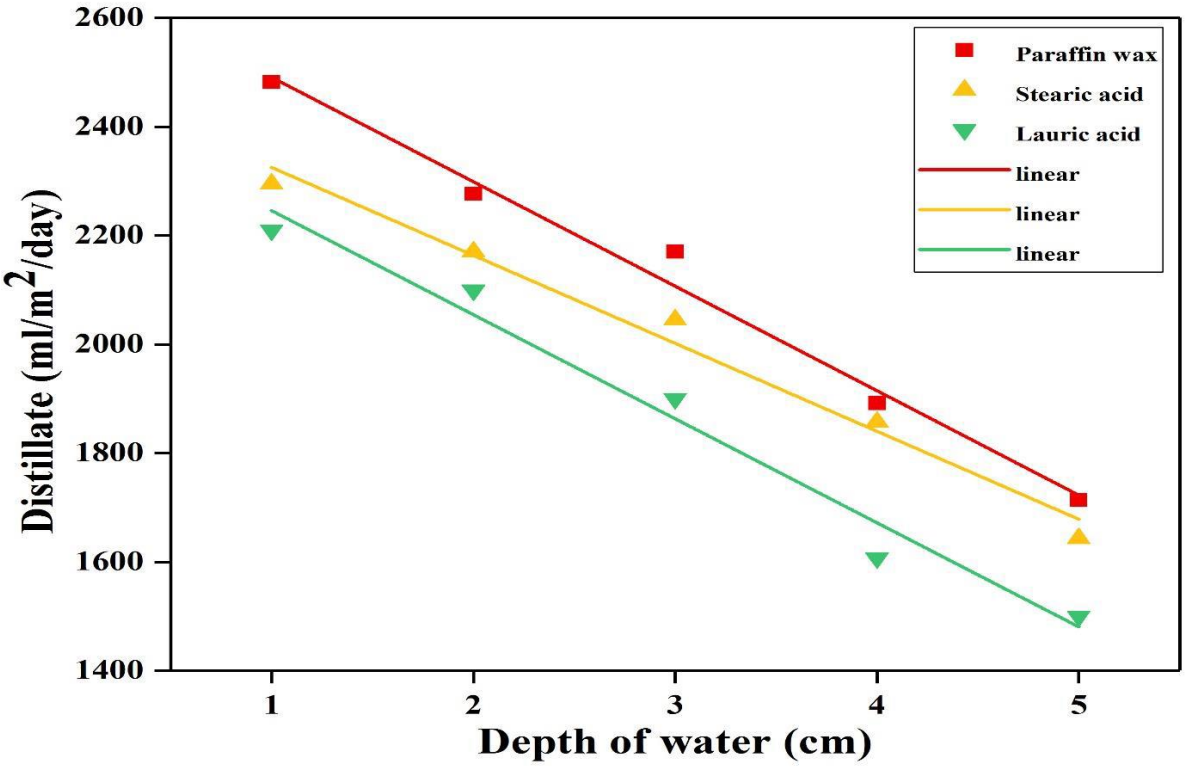


**Fig. 3.17** Variation of total distillate with depth of water

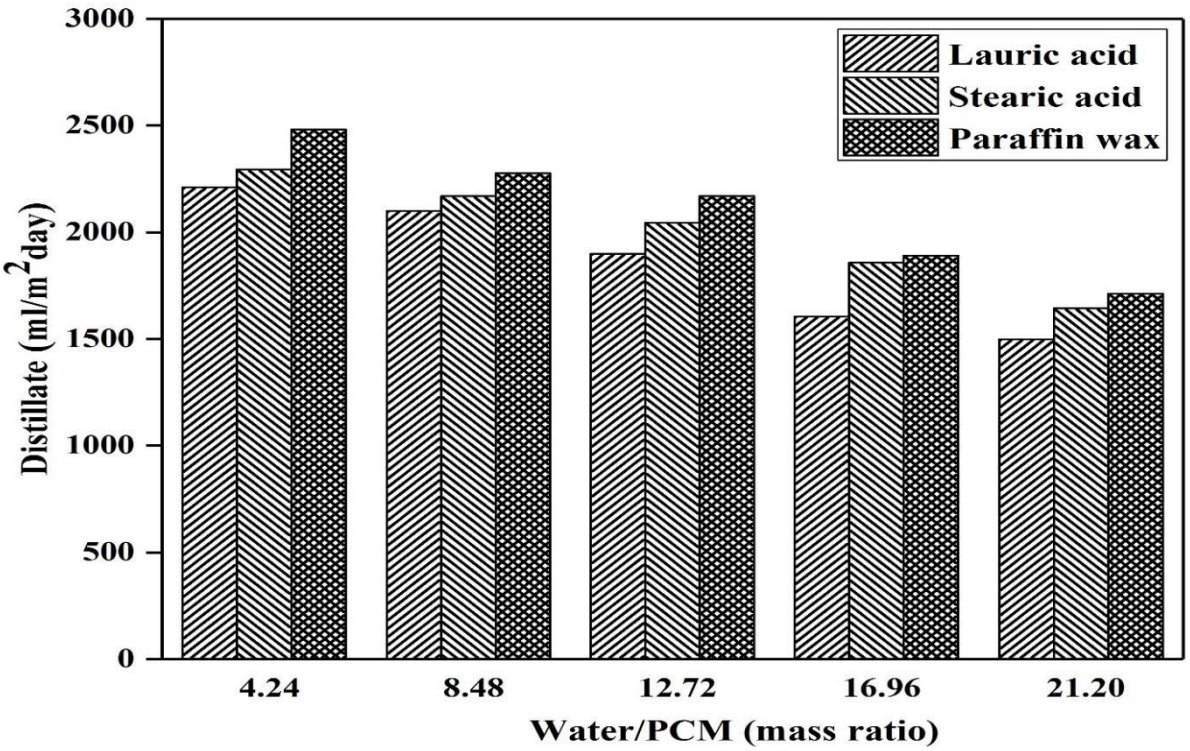


**Fig. 3.18** Variation of (daily yield) vs (water mass/PCM mass)

### 3.4.5 Variation of total distillate with water depth and validation

Fig. 3.17 indicates the daily total distillate at the different levels of water depth (1–5 cm) and Fig. 3.18 represents the total daily distillate versus mass ratio (Water/PCM). The maximum daily distillate obtained for paraffin wax, stearic acid, and lauric acid have been 2482, 2295, and 2210 ml/$m^2$-day, respectively. It can also be observed that maximum output has been obtained at 1 cm for all three PCMs. This was because as the water depth increases the amount of water in the basin increases leading to lower water temperature as shown in Figs. 3.7, 3.8, and 3.9. A clear trend can be asserted that with an increase in depth, total distillate decreases. Table 3.4 represents the parameters and linear equation obtained after the curve fitting of the experimental data. The curve fitting having $R^2$ and adjusted $R^2$ value greater than 0.95 is acceptable, suggesting that the obtained linear equation can explain 95% of the data variability (Bajar et al., 2016; Buratti et al., 2018). Pearson's r represents the relationship between X (water depth) and Y (distillate) variables. Its value lies between −1 to +1. As can be observed from Table 3.4 that all three curves, Pearson's r-value lie closed to −1, suggesting that Y

decreases when X increases. Fig. 3.19 represents the comparison of the increase in distillate due to PCM with the other two studies carried out by Arunkumar et al. (Arunkumar et al., 2013) and Tabrizi et al. (Tabrizi et al., 2010). In our study, total distillate without PCM has been 1298 ml/m$^2$-day at 1 cm depth Whereas, the increase in distillate due to PCM at 1 cm depth have been 1202 (paraffin wax), 1015 (stearic acid) and 930 (lauric acid) ml/m$^2$-day as compared to 940 (Arunkumar et al., 2013) and 290 ml/m$^2$-day (Tabrizi et al., 2010).

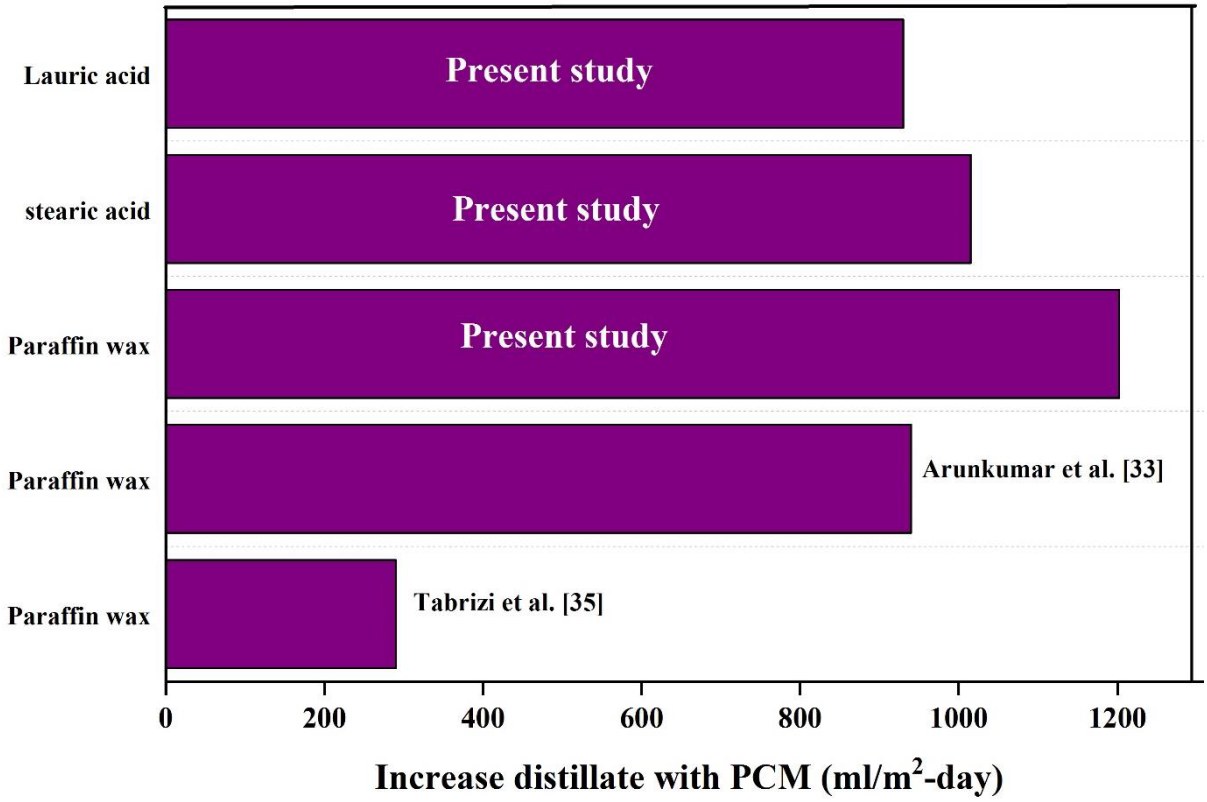


**Fig. 3.19** Comparison of increased distillate with PCM

It is quite clear that in our study the increase in distillate for paraffin wax and stearic acid has been found to be greater than the other two studies. However, giving major scope for regions with lower radiation and ambient temperature. This is due to the fact that lauric acid (42–46 $^{o}$C) has a much lower melting point as compared to paraffin wax (58–60 $^{o}$C) and stearic acid (52–56 $^{o}$C).

## 3.5 Summary

We have only used copper cylinders to keep PCMs whereas the other authors used spherical balls to keep the same. Since cylinders provide an enhanced surface area rather than sphere, our solar still renders better distillation outputs rather than the other authors due to its technological advantages attributed because of better heat transfer. The meteorological conditions of other authors have been found as almost similar. Copper cylinders filled with phase change materials integrated beneath the basin liner improved the overnight productivity of the solar still. Water basin temperature decreased with increase in water depth with paraffin wax being least effected due to high heat storing capacity as compared to stearic and lauric acid. Total distillate decreased linearly with the water depth in all three PCMs. Paraffin wax has the maximum distillate as compared to stearic acid and lauric acid.